Synchronization in a temporal multiplex neuronal hypernetwork

Sarbendu Rakshit, Bidesh K. Bera, and Dibakar Ghosh*
Physics and Applied Mathematics Unit, Indian Statistical Institute, 203 B. T. Road, Kolkata 700108, India

(Received 5 July 2018; published 14 September 2018)

Synchronization in time-varying complex dynamical systems has been explored in a variety of different coupling topologies during the last two decades. In most of the previous cases, the basic time-varying coupling topologies were considered to be a single interaction between the nodes or in a monolayer configuration, although in many real situations the types of interactions are more than one or in the form of multilayer. In this work, we study the synchronization in multiplex neuronal network, which evolves with time, and each layer consists of more than one interaction function. Specifically, we consider a neuronal hypernetwork at each layer in which neurons are communicated with each other via electrical and chemical synapses simultaneously and independently. The network corresponding to the electrical gap junctional coupling form a small-world network while the connection associated with the chemical synaptic interaction forms a unidirectional random network. Then intralayer connections are allowed to switch stochastically over time with a characteristic rewiring frequency, whereas interlayer connections via electrical synapses are time invariant. We explore the intralayer and interlayer neuronal synchrony in such network and analytically derive the necessary stability conditions for synchrony using master stability function approach, and excellently match with our numerical findings. Interestingly, we find that the higher frequency of switching links in the intralayer enhances both intralayer and interlayer synchrony and conferring larger windows of synchrony. We also analyze the robustness of these synchronization states with respect to initial conditions using the basin stability framework. Furthermore we find that rapidly changing networks take much less time to reach synchronization state. Lastly, we inspect the dynamical robustness of interlayer synchronization against stochastic demultiplexing of each replica, with analytical justification.

DOI: 10.1103/PhysRevE.98.032305

I. INTRODUCTION

The research on complex networks provides a good tool for better understanding the universal properties and various collective features, which appear through the interaction among the large number of dynamical units, ranging from biological systems to technological and social systems. Different types of interactions appear due to the depending on their nature of coupling mechanisms. The combination of different connection types and underlying network structures play a crucial role for proper functioning of the connecting unit. From the dynamical point of view, different types of interaction schemes can be figured out into various classes of network architectures.

The different class of network structures can be organized in a single network in which each class of networks effects the other networks and such architecture is named a multilayered network [1–3]. Generally, the multilayer network structure possesses two types of interactions, one is intralayer and another is interlayer interaction. The first type is defined as the interaction of nodes within the same layer, while the second type established the link between the nodes, which are located in different layers. It may consist of more than two different layers where the interaction within each layer may differ from other layers as well as layer-layer connections. When the layers are composed with the same number of nodes and the connection between the same nodes from the different layer are preserved, then the multilayered structures are termed as a multiplex network, where a given node in a layer is only connected to its counterpart nodes in the rest of the layers. The multilayered networks are assisted to better understand the various types of social interactions, from physical to online level. For instance, mobility networks [4] where each isolated unit may be served through the different types of transports, spreading of epidemic process, and social network [5] in which the people from one community are tied to and interact with the other communities by various types of relations, subway network [6], air transportation network [7], neuronal network [8,9], and also several real-world systems [1,2], all are captured in multilayered structure. In the neurosciences, how the functional brain activities are connected to their underlying interacting structural connectivity is a big issue. In the multilayer formation, such connection type may be suitably described by considering the one layer as structural connectivity layer and other is functional interaction layer [10]. Various types of natural phenomena, such as epidemic spreading [11–14], percolation [15,16] and diffusion process [17], evolutionary games [18], and controllability [19] were studied in the multilayered framework and have been found to be significantly different results from the monolayer case.

Recently, the study on hypernetworks [20], containing two or more network topologies corresponding to different interaction schemes, is an interesting topic of research. In this network, different interaction types are fully independent, i.e., the presence of connection between two nodes does not affect the other types of interactions between them. The interneuronal communication type is one of the best representations of

*dibakar@isical.ac.in

such network where the interaction between neurons happens through two different synapses, namely, the electrical gap junction and chemical synapses [21]. Another example, the coordination motion of the shoal of fish [22,23], where the coordination of each individual not only depends on their visual perception, but also they have chemical sensing in order to locate their mates with respect to the shoal. Also, the concept of interdependent network [25], networks of networks [24], and computer communication networks [25] all belong to the class of hypernetwork where the set of interacting nodes are connected to the other set of nodes with different modes for normal functioning.

Various types of nontrivial collective features emerge due to the presence of interactions in two or more dynamical systems, among them synchronization phenomenon is the more studied subject during the last few decades for its many applications in several physical and engineered systems [26]. In multilayered network structure, different types of synchronization have been investigated such as interlayer and intralayer synchronization [27–30], cluster synchronization [31], chimera states [32], and explosive synchronization [33]. In all these cases, the network structures are assumed to be time static, i.e., the underlying network architectures do not evolve with respect to time. However, in many realistic situations where the connection types are not stagnant, rather they are dynamic, structured, and time variant, which means the interactional arrangements are appeared, disappeared, or rewired at different time scale [34]. For example, the social interaction network [35], where the relationship between two communities or individuals are continuously created, changed, or terminated over time, person-to-person communication [36], temporal progression of the links in various neuronal and artificial networks [37]; all are time-varying features. In this context, significant attention has been devoted in the last decade for investigation of synchronization property in time-varying complex network [38–42], since the time-varying concept has lots of applications in many fields of science, which include power transmission systems [43], disease spreading [44], consensus problem [45], process of chemotaxis [46], protein-protein interaction, gene regulatory network [47], and functional brain network [48], etc.

Brain function depends on the communication between the neurons where the interaction happens through the electrical and chemical synapses. The coexistence of these two different types of synaptic communications were observed in most of the nervous systems and worked independently [21]. Such types of interactions' arrangement among the neurons are well understood by constructing a neuronal hypernetwork [49] and the time-varying interactions are inherent features of such hypernetwork as both the synaptic interactions change over time. The neuronal synchrony is one of the fundamental issues in the field of brain dynamics, since there are several types of abnormal patterns of synchronization in the brain, which are associated with the various types of brain disordered diseases [50] such as Parkinson's, Alzheimer's, epilepsy, and schizophrenia. Also in many neuronal systems such as human thalamocortical area, mammalian visual cortex, stomatogastric ganglion of the spiny lobster, and human cardiorespiratory system [51], the patterns of neuronal synchrony were detected experimentally [52–54]. Due to the presence of a large number of neurons in the neuronal network, the neurons are always performing with a subnetwork in which they are highly lumped and clotted within these subensembles and also several subpopulations are connected through different types of interactions for various biological processes. In this context, multilayered network structure is the best representation of such type of neuronal interaction. In most of the previous works, networks were investigated by considering either electrical or chemical synaptic communication in the monolayer case with static interaction scheme. The neuronal synchrony in the time-varying hypernetwork in the multilayer formation has not yet been studied, which has a great importance in the field of neuroscience and deserves significant attention.

Motivated by the above discussion, we study the complete neuronal synchrony in the time-varying multilayer hypernetwork where each node of the network is modeled with Hindmarsh-Rose (HR) neuronal oscillator. Here, we consider that each layer consists of two types of synaptic communications, bidirectional electrical coupling and unidirectional chemical synaptic interaction in which the connection associated with the electrical communication forms a small-world network while the links corresponding to the chemical synaptic interaction form a unidirectional random network. All the intralayer connections are allowed to vary with respect to time with a characteristic frequency, whereas interlayer connections are modeled by electrical coupling, which is stagnant. We analytically derive the necessary condition for intralayer and interlayer synchronization through master stability function (MSF) [55] approach and confirmed by numerical investigations. To quantify the stability of synchronized states in a global scene, we use the basin stability [30,56,57] framework.

The rest of the paper is organized in the following way. Section II introduces the general mathematical framework for temporal multilayer hypernetwork model. In Sec. III, we describe both types of synaptic communications and neuronal hypernetwork with multilayer architecture by taking the HR neuronal model. Section IV is devoted to our numerical results on intralayer and interlayer synchronization and global stability analysis using basin stability framework. The linear stability analysis of both synchronize states are analyzed in Sec. V by MSF approach. Section VI provides the robustness of the interlayer synchronization state under stochastic demultiplexing. Conclusions of our entire findings are in Sec. VII.

II. MATHEMATICAL MODEL OF THE TIME-VARYING MULTIPLEX HYPERNETWORK

We start by considering two layers where each layer is composed of N nodes of d-dimensional identical dynamical systems. The states of the layers are represented by the vectors $\mathbf{X} = \{\mathbf{x}_1, \mathbf{x}_2, \ldots, \mathbf{x}_N\}$ and $\mathbf{Y} = \{\mathbf{y}_1, \mathbf{y}_2, \ldots, \mathbf{y}_N\}$ with $\mathbf{x}_i, \mathbf{y}_i \in \mathbb{R}^d$ for $i = 1, 2, \ldots, N$. In our prescribed model, each of the layers interact through M different tiers of connections, which represent different kinds of couplings among themselves. The nodes for a particular layer interacting in each tier are precisely the same elements. Then, the dynamics of the entire system in layer-1 and layer-2 can be described,

respectively, as

$$\dot{\mathbf{x}}_i = F(\mathbf{x}_i) + \sum_{\alpha=1}^{M} \epsilon_\alpha \sum_{j=1}^{N} \mathscr{A}_{ij}^{(1,\alpha)}(t)\, G_\alpha(\mathbf{x}_i, \mathbf{x}_j) + \eta\, H(\mathbf{y}_i, \mathbf{x}_i),$$

and

$$\dot{\mathbf{y}}_i = F(\mathbf{y}_i) + \sum_{\alpha=1}^{M} \epsilon_\alpha \sum_{j=1}^{N} \mathscr{A}_{ij}^{(2,\alpha)}(t)\, G_\alpha(\mathbf{y}_i, \mathbf{y}_j) + \eta\, H(\mathbf{x}_i, \mathbf{y}_i), \tag{1}$$

where $F : \mathbb{R}^d \to \mathbb{R}^d$ and $H : \mathbb{R}^d \to \mathbb{R}^d$ are the continuously differentiable functions, which represent the autonomous evolution of the uncoupled oscillator and output vectorial function between the layers, respectively. Here $G_\alpha : \mathbb{R}^d \to \mathbb{R}^d$ be the vector field of the output vectorial function within the layers for the tier α. Parameter ϵ_α is the intralayer coupling strength for the tier α and η is the interlayer coupling strength. These intralayer network configurations are time varying, encoded by the adjacency matrices $\mathscr{A}^{(l,\alpha)}(t)$ for the tier α in the lth layer ($l = 1, 2$ and $\alpha = 1, 2, \ldots, M$). At time t, $\mathscr{A}_{ij}^{(l,\alpha)}(t) = 1$ if ith node and jth node of layer l are connected in the tier α and zero otherwise. Consider $\mathscr{L}^{(l,\alpha)}(t)$ to be the corresponding zero-row sum Laplacian matrices obtained from the adjacent matrices $\mathscr{A}^{(l,\alpha)}(t)$ with the diagonal elements $\mathscr{L}_{ii}^{(l,\alpha)}(t)$ are the sum of the corresponding rows of $\mathscr{A}^{(l,\alpha)}(t)$ and the off-diagonal elements are the negative of the corresponding elements in the adjacent matrices, i.e., $\mathscr{L}_{i,j}^{(l,\alpha)}(t) = -\mathscr{A}_{i,j}^{(l,\alpha)}(t) (i \neq j)$ and $\mathscr{L}_{i,i}^{(l,\alpha)}(t) = \sum_{j=1}^{N} \mathscr{A}_{i,j}^{(l,\alpha)}(t)$. Now the links of each tier in both the layers vary over time through the rewiring of each link in the entire network stochastically and independently, with characteristic rewiring frequency f, while the interlayer connections are preserved over time. Particularly, at any time t, given time step dt, we rewire each layer by constructing a new network independently, with probability $f\,dt$. Large f indicates very fast switching of links, implying that the networks change rapidly, whereas small f implies that the two layers are almost static, as the links have a very low probability of change.

A schematic diagram illustrating time-varying interactions in such a multilayer hypernetwork of $N = 10$ nodes and $M = 2$ different tiers of connections is shown in Fig. 1. By considering the distinct nature of the interactions, we construct two different types of interacting layers, one unidirectional random network and the other one is a bidirectional small-world network. The green solid line shows a small-world network of average degree 4 corresponding to the bidirectional coupling and the dashed red line shows the unidirectional random network with constant in-degree 1. The coexistence of these two networks constitutes a hypernetwork, with each tier generally having different links and representing a different kind of interaction. At two particular instances of time $t = t_1$ and $t = t_2$, the different interaction patterns, as reflected by different links, are shown in Figs. 1(a) and 1(b), respectively.

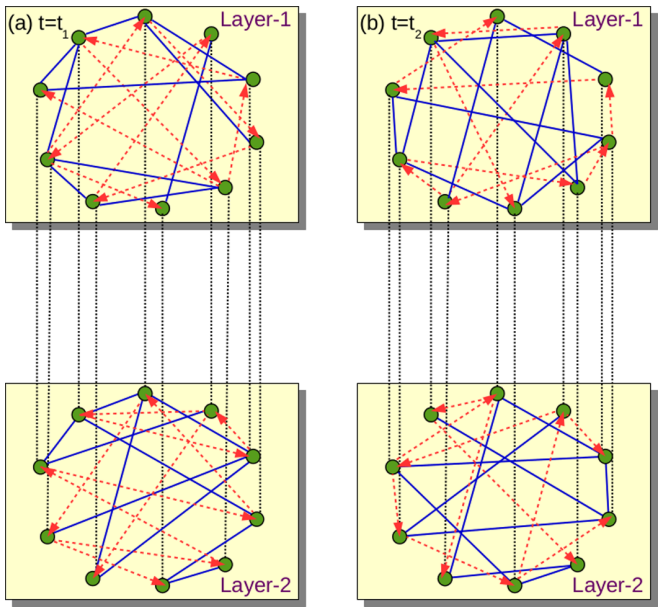

FIG. 1. Schematic representation of time-varying connections in a hypernetwork at two different time instants: (a) $t = t_1$ and (b) $t = t_2$. Each node is denoted by a gray solid circle. The red dashed lines denote unidirectional interactions, and forms a random network with constant in-degree 1, while the green solid lines represent bidirectional coupling, forming a small-world network of average degree 4.

III. TIME-VARYING MULTILAYER NEURAL HYPERNETWORK

A neuronal network is one of the most important examples of time-varying hypernetwork, as neurons interact through both electrical gap junctions, as well as chemical synapses, and these links are known to vary with time. These two types of synapses are elementary functional connections, which enable information to be swiftly transferred between neurons. Through a chemical synapse, a signal is conveyed chemically via neurotransmitter molecules such as Acetylcholine, gamma-Aminobutyric acid, dopamine, and serotonin, packaged inside small synaptic vesicles. In a probabilistic manner, neurotransmitters are released by exocytosis from a presynaptic neuron into the synaptic cleft. These molecules then bind to specific postsynaptic receptors in adjacent postsynaptic neuronal cells, leading to a unidirectional transmission of information. In this case the distance between presynaptic and postsynaptic ends may be large, approximately 20–40 nm [58] [see the schematic diagram Fig. 2(a)]. In electrical synapses, the cytoplasm of adjacent cells is directly connected by a channel called a gap junction. So direct bidirectional passage of electric current, calcium, cyclic AMP, and inositol-1,4,5 trisphosphate occurs between the presynaptic end and the postsynaptic neuron [cf. Fig. 2(b)]. Here the membranes of the presynaptic and postsynaptic neurons are extremely close to each other, approximately 3.5 nm [59]. So the electrical synapses are naturally bidirectional, and the signal transmission speed is much faster than chemical transmission. The electrical signal propagates through the membrane potential in two adjacent neuronal cells by making a gap junctional channel and it occurs bidirectionally. In the case of chemical synaptic interaction, the information passes chemically from presynaptic cell to postsynaptic cell and it always happens in a unidirectional manner. Both these types of synapses coexist during information processing in most of the nervous systems.

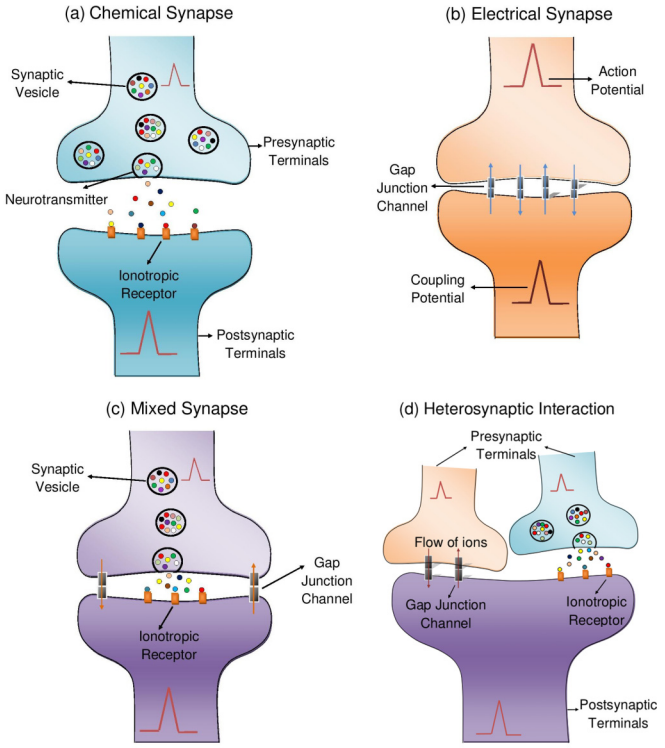

FIG. 2. Different types of neuronal interactions through electrical and chemical synapses. (a) Chemical transmission occurring unidirectionally through chemical synapses. (b) Bidirectional electrical communication intercedes by the electrical gap junction. (c) Mixed synaptic interaction: coexistence of both electric and chemical synaptic interactions eventuate between two neurons. (d) Heterosynaptic interaction: one neuron simultaneously coupled with two other neurons, one through the chemical synapse and the other through gap junction channel.

For interneuronal communication both types of coupling do not necessarily act simultaneously, rather they operate independently [21] over time. The coexistence of chemical and electrical synapses among two neurons is known as a mixed synapse [cf. Fig. 2(c)], while heterosynaptic interaction of a neuron is connected with two different neurons one by chemical synapse and another by electrical synapse [cf. Fig. 2(d)].

To represent the mathematical form of the above hypernetwork, we consider two layers where each layer is composed of N Hindmarsh-Rose neurons connected simultaneously by electrical and chemical synapses. Dynamics of the entire network can be described by

Layer-1:

$$\dot{x}_{1i} = y_{1i} - a x_{1i}^3 + b x_{1i}^2 - z_{1i} + I - \epsilon \sum_{j=1}^{N} \mathscr{L}_{ij}^{(1,e)}(t)\, x_{1j} + \frac{g_c}{k_c}(v_s - x_{1i}) \sum_{j=1}^{N} \mathscr{A}_{ij}^{(1,c)}(t)\, \Gamma(x_{1j}) + \eta(x_{2i} - x_{1i}),$$

$$\dot{y}_{1i} = c - d x_{1i}^2 - y_{1i},$$

$$\dot{z}_{1i} = r(s(x_{1i} - x_0) - z_{1i})$$

and Layer-2:

$$\dot{x}_{2i} = y_{2i} - a x_{2i}^3 + b x_{2i}^2 - z_{2i} + I - \epsilon \sum_{j=1}^{N} \mathscr{L}_{ij}^{(2,e)}(t)\, x_{2j} + \frac{g_c}{k_c}(v_s - x_{2i}) \sum_{j=1}^{N} \mathscr{A}_{ij}^{(2,c)}(t)\, \Gamma(x_{2j}) + \eta(x_{1i} - x_{2i}),$$

$$\dot{y}_{2i} = c - d x_{2i}^2 - y_{2i},$$

$$\dot{z}_{2i} = r(s(x_{2i} - x_0) - z_{2i}), \tag{2}$$

where $i = 1, 2, \ldots, N$ is the neuron index, N is the total number of neurons in each layer. Here x_{li} is the membrane potential of the i^{th} neuron, y_{li} is associated with the fast current (for example Na^+ or K^+), z_{li} with the slow Ca^{2+} current in the lth layer ($l = 1, 2$) and r modulates the slow dynamics of the system. The control parameters g_c and ϵ are strengths of the chemical and electrical synapses, respectively, which determine how much the information will distribute between neurons through the different coupling channels. η is the interlayer electrical coupling strength, that allows one to tune the strength of the interactions between two layers. We fix the parameters $a = 1, b = 3, c = 1, d = 5, r = 0.005, s = 4, x_0 = -1.6, I = 3.25$, for which an isolated system exhibits multi-time-scale chaotic spiking-bursting behavior of the membrane potential. With the above set of parameter values, the isolated system is monostable, i.e., there is no other multiple asymptotic states. The mechanism for the activation and deactivation of nonlinear chemical synapse is modeled by the sigmoidal input-output function $\Gamma(\mathbf{x}) = \frac{1}{1+\exp[-\lambda(\mathbf{x}-\Theta_s)]}$. The synaptic reversal potential is v_s, and for $v_s > x_{li}(t)$, the synaptic current has depolarizing effect making the synapse excitatory, and for $v_s < x_{li}(t)$, the synaptic current has a hyperpolarizing effect making the synapse inhibitory. For the chosen set of system parameters, $|x_{li}(t)| < 2$, thus $(x_{li}(t) - v_s)$ is always negative if $v_s = 2$, and so that the chemical synapse is excitatory forever, i.e., when the presynaptic neuron spikes, it induces the postsynaptic neuron to spike. The parameter λ determines the slope of the sigmoidal function and Θ_s is the synaptic firing threshold. Hereafter $\Theta_s = -0.25$ and $\lambda = 10$.

Here one neuron in a layer is connected to its replica on the other layer by the electrical synapse, i.e., the interlayer connection is diffusive type. The intralayer couplings are considered through two types of interactions: bidirectional electrical gap junctional coupling and the unidirectional chemical ion transportation through chemical synapses. The connectivity of the chemical synapses of layer l is considered to be a unidirectional random network, described by the adjacency matrix $\mathscr{A}^{(l,c)}(t)$, for $l = 1, 2$. The corresponding Laplacian matrices are given by $\mathscr{L}_{ij}^{(l,c)}(t) = -\mathscr{A}_{ij}^{(l,c)}(t)$ for $i \neq j$, and $\mathscr{L}_{ii}^{(l,c)}(t) = \sum_{j=1}^{N} \mathscr{A}_{ij}^{(l,c)}(t)$. The diverse in-degree of the nodes does not yield complete synchronization due to the nonexistence of the synchronization manifold. So to exist the intralayer synchronization, we have to consider identical in-degree k_c of each node in each layer for all time. Here in-degree k_c reflects the number of signals each neuron receives through chemical synapses. So, $\mathscr{L}_{ii}^{(l,c)}(t) = k_c$ and $A^{(l,c)}(t)$ are always nonsymmetric matrices. The Laplacian matrices corresponding to the electrical synaptic network

in the two layers are $\mathscr{L}^{(1,e)}(t)$ and $\mathscr{L}^{(2,e)}(t)$, respectively, which deliberated as small-world networks. These networks are constructed by following the procedure proposed by Watts and Strogatz [60]. We commence with N nodes with regular ring coupling topology, where each node is connected to its $2k$ nearest neighbors, k on each side. Then with probability p, we reconnect all the initial edges to vertices chosen uniformly at random from distant nodes, with dual edges impermissible. So the average degree of the electrical synaptic networks is $k_e = 2k$.

In addition, we consider the time-varying electrical and chemical synaptic connections for both the layers, which form a time-varying neuronal hypernetwork. The intralayer links in both the layers vary over time through the rewiring of each link in the entire network stochastically and independently, with an average frequency f, while the interlayer connections are preserved over time. At any time t, two networks corresponding to two synapses coexist in each layer and hence the four networks rewire with probability fdt, where dt is the integration time step. For the sake of simplicity, we take the rewiring frequency of the four networks in both the layers are identical. Particularly, at any time t, given time step dt, we rewire each network by constructing a new network, independently, with probability fdt. Now the successively created new networks will be statistically equivalent with the previous one due to choice of fixed identical parameters k_e, k_c, and p throughout the procedure. Large f implies that the networks change rapidly, whereas for small f the links have very low probability of change. In the unidirectional random network, if there is an edge from the node i to j, it will be rewired from node i to any another node excluding j with probability $(1 - \frac{k_c}{N-1})fdt$. In the small-world network, if there is an edge between two distant neighbors, it is rewired to one of the nearest-neighbor nodes with probability $(1-p)fdt$, and if there is an edge between two nearest neighbors, then with probability $pfdt$, it is replaced by a connection to a randomly chosen distant node.

In the following section, our main aim is to explore the effect of network's parameters, namely rewiring frequency f through which each link in each layer is rewired stochastically and independently, interlayer and intralayer coupling strengths η and ϵ on the emergence of intralayer and interlayer synchronization states. For that, we fix the local dynamics of each HR neuronal node in the chaotic spiking-bursting state. We integrate the Eq. (2) using fourth-order Runge-Kutta method with integration time step $dt = 0.01$ and random but fixed initial conditions from the phase space volume $[-1.5, 2.0] \times [-0.7, 1.0] \times [2.9, 3.4]$. To draw the following parameter regions, we have taken 20 network realizations at each point.

IV. NUMERICAL RESULTS AND GLOBAL STABILITY ANALYSIS

In the proposed multiplex hypernetwork (2), two distinctive forms of synchronization emerge, namely, intralayer and interlayer synchronization. Interlayer synchronization occurs when each unit in a given layer evolves synchronously with its replicas, regardless of whether or not it is synchronized with the other units of the same layer. Contrariwise, intralayer

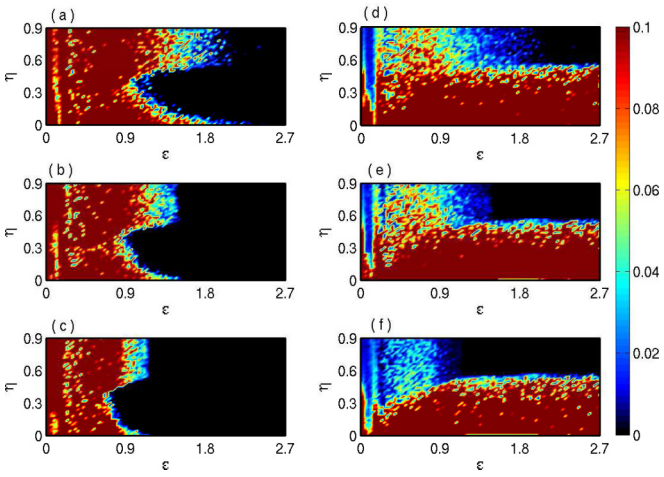

FIG. 3. Left and right panels represent the intralayer and interlayer synchronization error in (ϵ, η) parameter space with different values of $f = 0.001$ (top row), $f = 0.1$ (middle row), $f = 10.0$ (bottom row). Other parameters: $g_c = \frac{\epsilon}{2}, k_e = 6, k_c = 5$, and $p = 0.125$.

synchronization is defined as the state of synchrony in each of the individual layer, irrespective of the synchrony between the replica nodes. Here we delve into the intralayer and interlayer synchronization state of the temporal complex hypernetwork by changing the network parameters. The intralayer and interlayer synchronization errors are, respectively, defined as

$$E_{\text{intra}} = \lim_{T\to\infty} \frac{1}{T} \int_0^T \sum_{j=2}^{N} \frac{\|\mathbf{x}_j(t) - \mathbf{x}_1(t)\|}{N-1} dt, \tag{3}$$

and

$$E_{\text{inter}} = \lim_{T\to\infty} \frac{1}{T} \int_0^T \sum_{j=1}^{N} \frac{\|\mathbf{y}_i(t) - \mathbf{x}_i(t)\|}{N} dt, \tag{4}$$

where $\|\cdot\|$ denotes Euclidean norm and T is the long-time interval. To calculate the intralayer and interlayer synchronization errors, the time interval is taken over 1×10^5 units after an initial transient of 2×10^5 units.

The synchronization and desynchronization region are plotted in (ϵ, η) plane in Fig. 3 by taking several rewiring frequencies where color bar shows the variation of synchronization error. Here, chemical synaptic interaction strength $g_c = \frac{\epsilon}{2}$ is systematically varied with fixed average in-degree of the chemical synaptic network $k_c = 5$, SW probability $p = 0.125$ and average degree of the electrical synaptic network $k_e = 6$. The intralayer synchronization regions are shown by simultaneously varying ϵ and η in the left panel [Figs. 3(a)–3(c)]. For lower rewiring frequency $f = 0.001$, that is, when intralayer connections are almost static over time, higher intracoupling strength is needed for complete neuronal synchrony in both the layers in presence or absence of interlayer connection, result illustrated in Fig. 3(a). When the rewiring frequency is increased at $f = 0.1$ and $f = 10.0$, then more enhancement of neuronal synchrony is observed (black region), presented in Figs. 3(b) and 3(c), respectively. Interestingly, in presence of interlayer interaction, mixed types of intralayer synchronization transition are observed, that is, first enhancement

of intralayer synchronization appears up to certain values of $\eta = 0.4$. Beyond that interlayer coupling strength, deenhancement of intralayer synchronization happens up to a critical threshold of ϵ and this scenarios is occurred in all exemplify values of the rewiring frequency f [Figs. 3(a)–3(c)]. Also note that, after certain value of $\eta = 0.55$, interlayer interaction does not have any effect on intralayer synchronization and is fully determined of ϵ for all respective values of rewiring frequencies. The right panel of Fig. 3 represents the interlayer synchronization regions in (ϵ, η) plane for different values of rewiring frequencies f. For lower switching case, i.e., $f = 0.001$, the interlayer synchronization region (black color) is small [Fig. 3(d)] compared to the slightly higher switching case as $f = 0.1$ in Fig. 3(e). Further rapid changing in the networks for $f = 10.0$ leads to the larger windows of the interlayer neuronal synchrony, depicted in Fig. 3(f). So from this figure, it is clear that more rapid changing of the networks leads to the enhancement of the both types of the neuronal synchrony while the presence of the interlayer connection induced the mixed type (enhancement and deenhancement) of intralayer synchronization transitions in the time-varying multilayer hypernetwork.

Now we analyze the global stability of these intralayer and interlayer synchronization states using basin stability (BS) measurement, which is a global nonlinear measure of stability that can be freely employ to any high-dimensional complex systems. It focuses on the volume of the basin of attraction, and a robust gadget for quantifying different multistable states. The algorithm for numerically computing BS is a highly practicable calculating algorithm with a cross-validation procedure. Our considered individual HR system is monostable in the local dynamics, so the destruction of the stable synchronization state due to bistability (or multistability) [61] will not be effected here. We integrate the entire system with sufficiently large number T of initial conditions, which are drawn randomly from the phase space volume. Let finally M be the number of initial conditions for which the desired synchronous state arrive. Then our desired BS for synchronous state is approximately $\frac{M}{T}$. Clearly the value of BS is bounded in the range [0,1]. The completely unstable synchronized state corresponds to $BS = 0$. When $BS = 1$, the entire basin of attraction will support the synchronized state, suggesting a globally stable state. Whereas $0 < BS < 1$ corresponds to the probability of getting the synchronous state form any randomly chosen initial state from the phase volume. Here we sample the phase space volume $[-1.5, 2.0] \times [-7.0, 1.0] \times [2.9, 3.4]$, and the final state is considered as synchronized if the corresponding synchronization error is less than 10^{-6}, otherwise the system is in a desynchronized state.

The BS of the complete neuronal synchronization is shown in (ϵ, η) parameter plane in Fig. 4 corresponding to Fig. 3. The color bar denotes the variation of BS for the quantification of global stability of the synchronization state. The deep blue color indicating the BS value as $BS \sim 0$, which implies that choosing any random initial condition from the prescribed basin volume always produces the incoherent dynamics. The deep red color corresponds to the $BS \sim 1$, which means that the full basin volume support gives rise to the synchronized states. The intermediate colors of the bar are

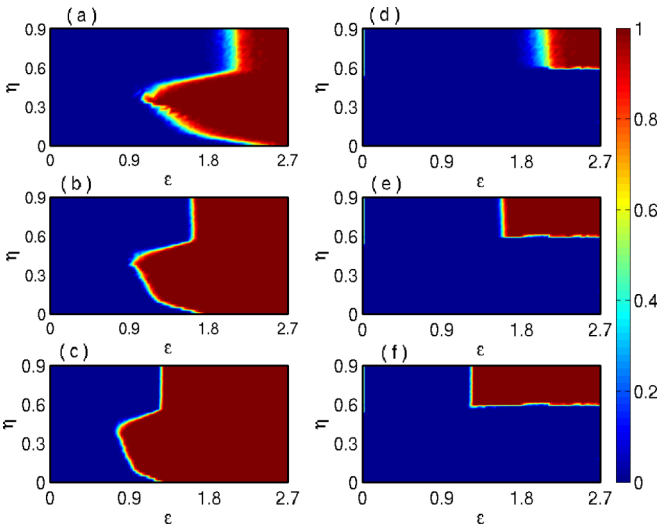

FIG. 4. Basin stability of intralayer (left) and interlayer (right) synchronization in (ϵ, η) parameter space with different values of $f = 0.001$ (top), $f = 0.1$ (middle), $f = 10.0$ (bottom). Other parameters are same as in Fig. 3.

associated with $0 < BS < 1$, signifying the coexistence of the desynchronized and synchronized states. The left and right panels of the Fig. 4 represent the BS of the intralayer and interlayer synchronized states with different rewiring frequencies at $f = 0.001, 0.01$, and 10.0. The enhancement of the synchronization region in (ϵ, η) parameter space with the increasing values of the rewiring frequencies is also reflected in Fig. 4 as same as in Fig. 3. Interestingly, we observe that the coexistence of synchronized and desynchronized regions is decreases with the increasing values of the rewiring frequencies and for sufficient fast switched links, there is a sharp transition from incoherent to coherent state.

Now we explore the intralayer and interlayer synchronized states in (f, ϵ) parameter space with systematically varying the chemical synaptic strength $g_c = \frac{\epsilon}{2}$ and interlayer interaction strength $\eta = \frac{\epsilon}{3}$. Intralayer and interlayer synchronized regions (black color region) are shown in left and right panels of Fig. 5, respectively, for two different average degrees $k_e = 4$ (top row) and $k_e = 6$ (bottom row) of the SW network corresponding to the electrical synaptic communication in the neuronal hypernetwork. The desynchronized and synchronized regions are characterized through the synchronization error whose variations are shown in the color bar. The larger synchronization area is observed for higher average degree of SW network of intra- as well as interlayer synchronization states. The higher rewiring frequencies give rise to the enhancement of both types of synchronization states. In intralayer synchronization case, discontinuous transition is observed. In Fig. 3, we observe first enhancement and then deenhancement of the intralayer synchronization because of the parameter η. Now along $\eta = \frac{\epsilon}{3}$ line it first enters to the synchronization region initially from the incoherent region, again the desynchronization region, and finally the synchronization region. This leads to the discontinuous transition of the intralayer synchronization in (f, ϵ) space. In Fig. 5(a) for $f \in (0.16, 30)$ after the occurrence of intralayer coherence it

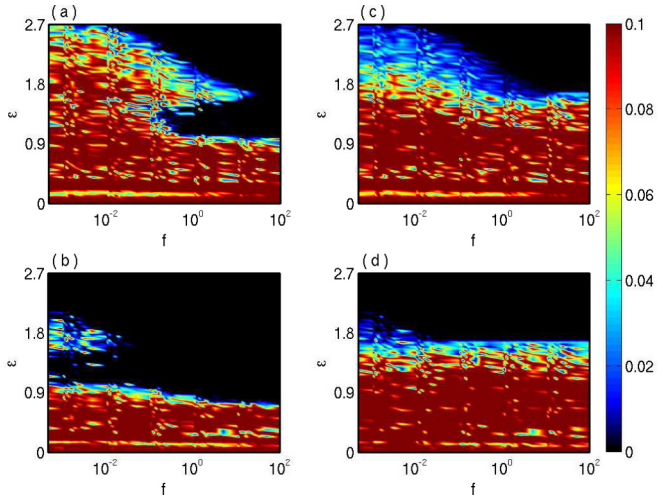

FIG. 5. Left and right panels represent the synchronization error of intralayer and interlayer synchronization in (f, ϵ) parameter space with $g_c = \frac{\epsilon}{2}$ and $\eta = \frac{\epsilon}{3}$. Here $k_c = 5$ and $p = 0.125$ ($k_e = 4$ for top panel, $k_e = 6$ for bottom panel).

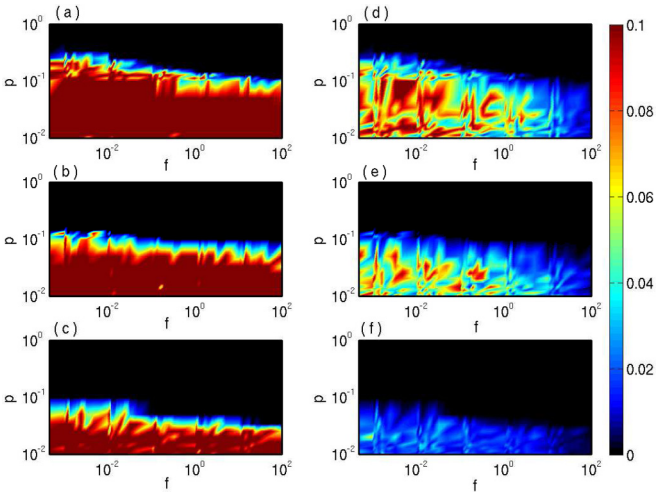

FIG. 7. (Left) intralayer and (right) interlayer synchronization error in (f, p) parameter plane. For $k_e = 4, \epsilon = 1.8$ (top row), $k_e = 6, \epsilon = 1.8$ (middle row), $k_e = 6, \epsilon = 2.7$ (bottom row). Other parameters: $k_c = 5$, $g_c = \frac{\epsilon}{2}$, and $\eta = \frac{\epsilon}{3}$.

again goes to incoherent as ϵ increases after further increased values enhancement of intralayer synchrony again happens. For higher average degree $k_e = 6$, this type of discontinuous transition occurs in a very narrow region for $f \in (0.005, 0.04)$ in Fig. 5(b). For interlayer synchrony, strictly monotonic enhancement is observed in (f, ϵ) plane for $k_e = 4$, but it is almost homogeneous for $k_e = 6$. The scenarios are displayed in Figs. 5(c) and 5(d).

The robustness of initial conditions on the complete neuronal synchronized state is investigated using the BS framework in Fig. 6 by simultaneous changes of parameters f and ϵ for two fixed values of degree of electric synaptic network k_e. The BS of intralayer and interlayer synchronized states are plotted in Figs. 6(a) and 6(b) and Figs. 6(c) and 6(d) respectively, with average degree of SW network $k_e = 4$ (top panel) and $k_e = 6$ (bottom panel) with fixed chemical in-degree $k_c = 5$. Here BS characterized the larger average degree leads to the more enlargement of the synchronized regions in (f, ϵ) parameter space. In the region of mixed type transition in (f, ϵ) plane of intralayer synchronized states, BS measure indicates the larger coexistence region of synchronized and desynchronized states while a narrow coexistence region is observed in interlayer synchronous state. Also note that the more coexistence regions of synchronized and desynchronized states are appeared in slow switching case while rapid changing links in the network bring on to the sharp transition from desynchronous to synchronous state, which reflects on the both types of synchronization states.

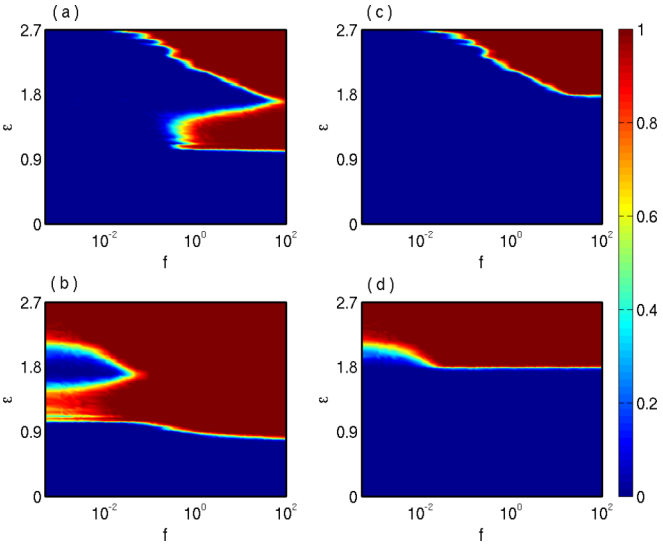

FIG. 6. The BS measure of intralayer (left) and interlayer (right) synchronization in (f, ϵ) parameter space for $k_e = 4$ (top) and $k_e = 6$ (bottom). The other parameters are same as in Fig. 5.

Next we investigate the emergence of synchrony in the neuronal hypernetwork with the interplay of SW probability p and rewiring frequency f. The smaller values of p represent the regular network topology, near unit value they represent the complete random network, and for certain intermediate values of p, it denotes the SW topology. Here we show the effect of continuous variation of the p and f on intralayer and interlayer synchronization states. Color bar of Fig. 7 shows the variation of the synchronized error by simultaneous changing of f and p. The black region of Figs. 7(a)–7(c) and 7(d)–7(f) represent the intra- and interlayer synchronization states in (f, p) parameter plane. Top, middle, and bottom panels for different average degree of SW network and synaptic strength as $k_e = 4, \epsilon = 1.8$; $k_e = 6, \epsilon = 1.8$, and $k_e = 6, \epsilon = 2.7$, respectively. Average in-degree of chemical synaptic network $k_c = 5$ is fixed, chemical synaptic interaction $g_c = \frac{\epsilon}{2}$ and interlayer coupling strength $\eta = \frac{\epsilon}{3}$. The intralayer and interlayer synchronization regions are smaller when the hypernetwork possesses lower average degree of the electrical synaptic network and the results are shown in Figs. 7(a) and 7(d), respectively. However, when average degree of SW network is increased at $k_e = 6$, then larger synchronous area in (f, p) plane are seen in Figs. 7(b) and 7(e) compare to Figs. 7(a) and

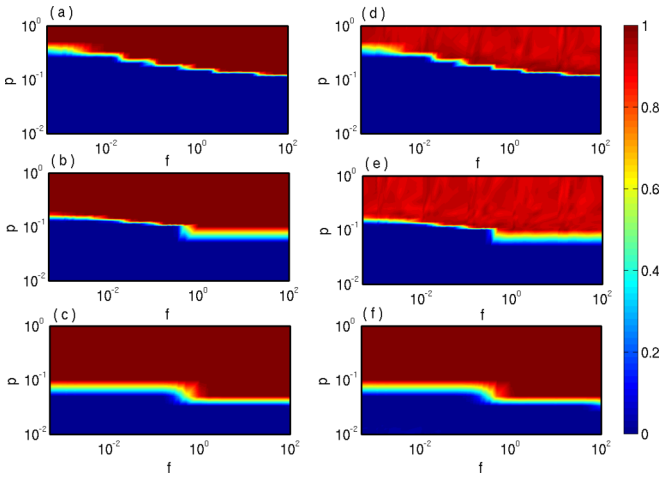

FIG. 8. BS for intralayer (left) and interlayer (right) synchronization in (f, p) parameter space corresponding to Fig. 7.

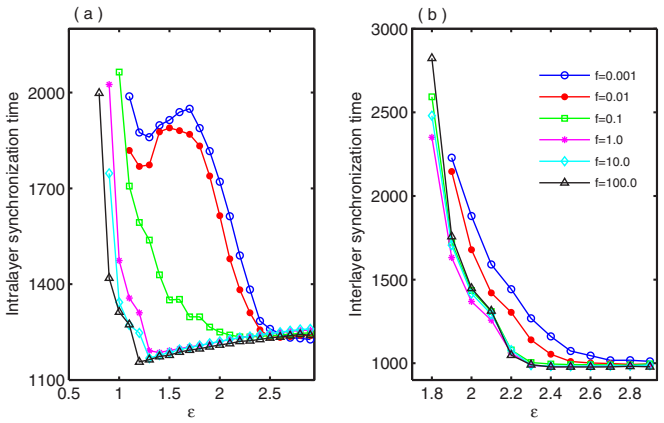

FIG. 9. (a) Intralayer and (b) interlayer synchronization time with respect to ϵ for different rewiring frequencies. Other parameters: $g_c = \frac{\epsilon}{2}$, $\eta = \frac{\epsilon}{3}$, $k_e = 6$, $k_c = 5$, $p = 0.125$.

7(d). Further increasing the value of synaptic strength $\epsilon = 2.7$ with $k_e = 6$, the critical threshold of p reduced and more larger synchronous region are observed in (f, p) parameter space in Figs. 7(c) and 7(f) for both intralayer and interlayer synchronization states. From this figure it is clearly shown that rapid switching of the intralayer links leads to the enhancement of the SW probability p for synchronization states irrespective values of the average degree of the bidirectional electrical communication network. Also, the transition from intralayer and interlayer synchronization states in (f, p) plane is nearly horizontal, which implies that p is independently determine the synchronization states for certain k_e and k_c.

Using BS measurement, the global stability of the intralayer and interlayer synchronization states are explored in Fig. 8. For most of these figures, there are a multistable regions of synchronized-desynchronized state in the transition area, especially for lower rewiring frequency. In Figs. 8(d) and 8(e) there is a significantly more bistable area beyond the transition point.

We evaluate average synchronization time by taking 50 network realizations. The intralayer and interlayer synchronization time are shown in Figs. 9(a) and 9(b), respectively, changing the synaptic strength for several representative values of rewiring frequency f. For $f = 0.001$ and $f = 0.01$, there is a mixed type behavior for intralayer synchronization time. It increases for some intermediate range of ϵ, in the exterior of that range it decreases. This happens due to the emergence of coexistence of synchronous and desynchronous state for those values of ϵ in Fig. 6(b). Also note that the higher rewiring frequency trends to minimize the synchrony time against the lower coupling values. Whereas interlayer synchronization time strictly decreases by increasing synaptic strength ϵ. From this figure (Fig. 9), it is clear that rapidly switching intralayer connections lead to decreases in the intralayer synchronization time by enhancing the critical synaptic coupling threshold. Interestingly, intralayer synchronization time increases with respect to higher coupling values, after reaching the minimal synchrony time. However, interlayer synchronization time is minimum at lower coupling strength for fast switching links in the network and for sufficiently large coupling values, interlayer synchronization time is saturated irrespective values of the rewiring frequencies.

V. LINEAR STABILITY ANALYSIS

This section is devoted to the linear stability analysis for the intralayer and interlayer synchronization in the multiplex hypernetwork given by Eq. (2) using MSF approach. It was reported that a time-varying network could be approximated by the time-averaged network for sufficiently fast rewiring. So we approximate our time-varying multilayer hypernetwork by a time-averaged static multilayer hypernetwork, for sufficiently fast switching. Then there exists a constant T (sufficiently large) such that

$$\bar{\mathscr{L}}^{(lc,le)} = \frac{1}{T}\int_t^{t+T} \mathscr{L}^{(lc,le)}(\tau)\, d\tau, \quad l = 1, 2, \tag{5}$$

with the time-averaged network and the rapidly varying network yielding the same synchronization transition, for sufficiently fast switching [62]. Since the topologies of the chemical synaptic networks in both the layers are same, their time-averaged adjacency matrices will be identical. For the similar reason, the time-averaged adjacency matrices of the electrical synaptic networks for both the layers will be also identical. Let $\bar{\mathscr{A}}^{(c)}$ be the time-averaged adjacency matrix of the chemical synaptic networks for the two layers, with $\sum_{j=1}^{N} \bar{\mathscr{A}}_{ij}^{(c)} = d_i^{(c)}$ $(i = 1, 2, \ldots, N)$ and $\bar{\mathscr{D}}^{(c)} = \mathrm{diag}(d_1^{(c)}, d_2^{(c)}, \ldots, d_N^{(c)})$; $\bar{\mathscr{L}}^{(c)}$ & $\bar{\mathscr{L}}^{(e)}$, respectively, be the time-averaged Laplacian matrices of the network for chemical and electrical synapses for both layers, with respective set of eigenvalues $\{0 = \gamma_1^{(c)}, \gamma_2^{(c)}, \ldots, \gamma_N^{(c)}\}$ and $\{0 = \gamma_1^{(e)}, \gamma_2^{(e)}, \ldots, \gamma_N^{(e)}\}$. Also consider that $V^{(c)}$ be the matrix of eigenvector of $\bar{\mathscr{L}}^{(c)}$. The entries of $\bar{\mathscr{L}}^{(c)}$ for both the layers are

$$\bar{\mathscr{L}}_{ij}^{(c)} = -\frac{k_c}{N-1} \quad \text{for } i \neq j,$$
$$= k_c \quad \text{for } i = j. \tag{6}$$

Also the entities of time-averaged networks of the electrical synapses are

$$\begin{aligned}\bar{\mathscr{L}}_{ij}^{(e)} &= -(1-p) \quad \text{for } i-k \leqslant j \leqslant i+k \text{ and } i \neq j,\\ &= k_e \quad \text{for } i = j,\\ &= -\frac{k_e\, p}{N-k_e-1} \quad \text{otherwise.}\end{aligned} \tag{7}$$

Taking time-averaged electrical and chemical synaptic networks for both the layers, the time-averaged system corresponding to the system (2) can be written as

$$\begin{aligned}\dot{x}_{1i} &= f(x_{1i}, y_{1i}, z_{1i}) - \epsilon \sum_{j=1}^{N} \bar{\mathscr{L}}_{ij}^{(e)} x_{1j} + \frac{g_c}{k_c}(v_s - x_{1i}) \sum_{j=1}^{N} \bar{\mathscr{A}}_{ij}^{(c)} \Gamma(x_{2j}) + \eta(x_{2i} - x_{1i}),\\ \dot{y}_{1i} &= g(x_{1i}, y_{1i}, z_{1i}), \quad \dot{z}_{1i} = h(x_{1i}, y_{1i}, z_{1i}),\\ \dot{x}_{2i} &= f(x_{2i}, y_{2i}, z_{2i}) - \epsilon \sum_{j=1}^{N} \bar{\mathscr{L}}_{ij}^{(e)} x_{2j} + \frac{g_c}{k_c}(v_s - x_{2i}) \sum_{j=1}^{N} \bar{\mathscr{A}}_{ij}^{(c)} \Gamma(x_{1j}) + \eta(x_{1i} - x_{2i}),\\ \dot{y}_{2i} &= g(x_{2i}, y_{2i}, z_{2i}), \quad \dot{z}_{2i} = h(x_{2i}, y_{2i}, z_{2i}),\end{aligned} \tag{8}$$

where, $i = 1, 2, \ldots, N$; $f(x, y, z) = y - ax^3 + bx^2 - z + I$, $g(x, y, z) = c - dx^2 - y$, $h(x, y, z) = r[s(x - x_0) - z]$. Notice that each neuronal oscillators are identical in the time-averaged network and coupled by bidirectional electrical and chemical synapses. The evolution and interaction dynamics all are continuous and differentiable. So the stability criterion for synchronization can be found through the MSF formalism, which gives the necessary condition for the stability of the synchronous solution.

A. Intralayer synchronization

When intralayer synchronization occurs, let layer-1 evolve synchronously with synchronization manifold $[x_{1i}(t), y_{1i}(t), z_{1i}(t)] = [x_1(t), y_1(t), z_1(t)]$ and for layer-2, $[x_{2i}(t), y_{2i}(t), z_{2i}(t)] = [x_2(t), y_2(t), z_2(t)]$, $\forall\, i = 1, 2, \ldots, N$. Now, at time t, perturb the ith node of layer-1 from its synchronization manifold with small amount $[\delta x_{1i}(t), \delta y_{1i}(t), \delta z_{1i}(t)]$ and the amount of perturbation for the ith node of layer-2 is $[\delta x_{2i}(t), \delta y_{2i}(t), \delta z_{2i}(t)]$. So, the current state of the i^{th} node for each layer can be written as

Layer-1: $(x_{1i}, y_{1i}, z_{1i}) = (x_1 + \delta x_{1i}, y_1 + \delta y_{1i}, z_1 + \delta z_{1i})$,

Layer-2: $(x_{2i}, y_{2i}, z_{2i}) = (x_2 + \delta x_{2i}, y_2 + \delta y_{2i}, z_2 + \delta z_{2i})$.

Now considering small perturbations and expanding around the intralayer synchronous solution up to first order, we obtain linearized equations of the error systems for layer-1 as

$$\begin{aligned}\delta\dot{x}_{1i} &= f_x(x_1, y_1, z_1)\delta x_{1i} + f_y(x_1, y_1, z_1)\delta y_{1i} + f_z(x_1, y_1, z_1)\delta z_{1i} - \epsilon \sum_{j=1}^{N} \bar{\mathscr{L}}_{ij}^{(e)} \delta x_{1j} - g_c \Gamma(x_1)\delta x_{1i}\\ &\quad + \frac{g_c}{k_c}(v_s - x_1)\Gamma_x(x_1)\left[k_c \delta x_{1i} - \sum_{j=1}^{N} \bar{\mathscr{L}}_{ij}^{(c)} \delta x_{1j}\right] + \eta(\delta x_{2i} - \delta x_{1i}),\\ \delta\dot{y}_{1i} &= g_x(x_1, y_1, z_1)\delta x_{1i} + g_y(x_1, y_1, z_1)\delta y_{1i} + g_z(x_1, y_1, z_1)\delta z_{1i},\\ \delta\dot{z}_{1i} &= h_x(x_1, y_1, z_1)\delta x_{1i} + h_y(x_1, y_1, z_1)\delta y_{1i} + h_z(x_1, y_1, z_1)\delta z_{1i}, \quad i = 1, 2, \ldots, N,\end{aligned} \tag{9}$$

where $f_x(x, y)$ denotes the partial derivative with respect to x. Similarly, the linearized equations for layer-2 are

$$\begin{aligned}\delta\dot{x}_{2i} &= f_x(x_2, y_2, z_2)\delta x_{2i} + f_y(x_2, y_2, z_2)\delta y_{2i} + f_z(x_2, y_2, z_2)\delta z_{2i} - \epsilon \sum_{j=1}^{N} \bar{\mathscr{L}}_{ij}^{(e)} \delta x_{2j} - g_c \Gamma(x_2)\delta x_{2i}\\ &\quad + \frac{g_c}{k_c}(v_s - x_2)\Gamma_x(x_2)\left[k_c \delta x_{2i} - \sum_{j=1}^{N} \bar{\mathscr{L}}_{ij}^{(c)} \delta x_{2j}\right] + \eta(\delta x_{1i} - \delta x_{2i}),\\ \delta\dot{y}_{2i} &= g_x(x_2, y_2, z_2)\delta x_{2i} + g_y(x_2, y_2, z_2)\delta y_{2i} + g_z(x_2, y_2, z_2)\delta z_{2i},\\ \delta\dot{z}_{2i} &= h_x(x_2, y_2, z_2)\delta x_{2i} + h_y(x_2, y_2, z_2)\delta y_{2i} + h_z(x_2, y_2, z_2)\delta z_{2i}, \mathrm{1} = 1, 2, \ldots, N.\end{aligned} \tag{10}$$

Now, three out of $3N$ Lyapunov exponents of system (9) are parallel to the intralayer synchronization manifolds of layer-1, remaining $3N - 3$ Lyapunov exponents are directed to the transverse direction to it. On the other hand, layer-1 will be

synchronized if all the Lyapunov exponents transverse to the synchronize manifolds are negative, also similarly for layer-2. So to find out $3N-3$ transverse Lyapunov exponents of systems (9) and (10) for layer-1 and layer-2, we project the perturbation vectors $(\delta x_{1i}, \delta y_{1i}, \delta z_{1i})$ and $(\delta x_{2i}, \delta y_{2i}, \delta z_{2i})$ on to the Laplacian eigenvector $V^{(c)}$ of the chemical synaptic layer. Since the Laplacian eigenvectors are always form a basis of $\mathbb{R}^N$, the choice of the layer is fully arbitrary. Then under this transformation, $(\delta x_{li}, \delta y_{li}, \delta z_{li})$ transforms to $(\sum_{j=1}^{N} V_{ij}^{(c)} \delta x_{lj}, \sum_{j=1}^{N} V_{ij}^{(c)} \delta y_{lj}, \sum_{j=1}^{N} V_{ij}^{(c)} \delta z_{lj}) = (\xi_{li}^{(x)}, \xi_{li}^{(y)}, \xi_{li}^{(z)})$ (say), $l = 1, 2$. Clearly this transformation is a linear transformation and since Rank $(V^{(c)}) = N$, it is an isomorphism. Hence when $(\delta x_{li}, \delta y_{li}, \delta z_{li})$ becomes (0,0,0), $(\xi_{li}^{(x)}, \xi_{li}^{(y)}, \xi_{li}^{(z)})$ will also becomes (0,0,0), and vice versa, for $l = 1, 2$. So the original error system (9) is equivalent to the transformed error system. Now, the dynamics of $\xi_{1i}^{(x)}$ becomes

$$\dot{\xi}_{1i}^{(x)} = f_x(x_1, y_1, z_1)\xi_{1i}^{(x)} + f_y(x_1, y_1, z_1)\xi_{1i}^{(y)} + f_z(x_1, y_1, z_1)\xi_{1i}^{(z)} - \epsilon \sum_{j=1}^{N} V_{ij}^{(c)} \sum_{k=1}^{N} \bar{\mathscr{L}}_{jk}^{(e)} \delta x_{1k} - g_c \Gamma(x_1)\xi_{1i}^{(x)}$$

$$+ g_c(v_s - x_1)\Gamma_x(x_1)\xi_{1i}^{(x)} - \frac{g_c}{k_c}(v_s - x_1)\Gamma_x(x_1) \sum_{j=1}^{N} V_{ij}^{(c)} \sum_{k=1}^{N} \bar{\mathscr{L}}_{jk}^{(c)} \delta x_{1k} + \eta\left(\xi_{2i}^{(x)} - \xi_{1i}^{(x)}\right). \tag{11}$$

Each column $V_i^{(c)}$ is an eigenvector of $\bar{\mathscr{L}}^{(c)}$, i.e., $\sum_{j=1}^{N} \bar{\mathscr{L}}_{ij}^{(c)} V_{ij}^{(c)} = \gamma_i^{(c)} V_i^{(c)}$. So,

$$\sum_{j=1}^{N} V_{ij}^{(c)} \sum_{k=1}^{N} \bar{\mathscr{L}}_{jk}^{(c)} \delta x_{1k} = \sum_{k=1}^{N} \sum_{j=1}^{N} V_{ij}^{(c)} \bar{\mathscr{L}}_{kj}^{(c)} \delta x_{1k} = \sum_{k=1}^{N} \gamma_i^{(c)} V_{ik}^{(c)} \delta x_{1k} = \gamma_i^{(c)} \xi_{1i}^{(x)}. \tag{12}$$

Let $V^{(e)}$ be the matrix of eigenvectors of $\bar{\mathscr{L}}^{(e)}$, the average Laplacian of the electrical synaptic network, with eigenvalue diagonal matrix $D^{(e)}$. Since Laplacian matrices are real symmetric, their eigenvectors are orthonormal, i.e., $V^{(c,e)} V^{(c,e)^{tr}} = I_N$. This gives

$$\bar{\mathscr{L}}^{(e)} V^{(e)} = D^{(e)} V^{(e)} \Rightarrow \bar{\mathscr{L}}^{(e)} = V^{(e)} D^{(e)} V^{(e)^{tr}} \Rightarrow \bar{\mathscr{L}}_{ij}^{(e)} = \sum_{r=1}^{N} V_{ri}^{(e)} \gamma_r^{(e)} V_{rj}^{(e)}. \tag{13}$$

Now $(\xi_{11}^{(x)}, \xi_{12}^{(x)}, \ldots, \xi_{1N}^{(x)})^{tr} = V^{(c)^{tr}} (\delta x_{11}, \delta x_{12}, \ldots, \delta x_{1N})^{tr}$ gives the projection of the synchronization error as

$$\delta x_{1i} = \sum_{k=1}^{N} V_{ki}^{(c)} \xi_{1k}^{(x)}, \tag{14}$$

where tr denotes the transpose of a matrix. Consider $U^{(e)} = V^{(e)^{tr}} V^{(c)}$, which adequately captures the association of the Laplacian eigenvectors of the electrical synaptic layer with the chemical synapses, and gives $U_{ij}^{(e)} = \sum_{k=1}^{N} V_{ik}^{(e)} V_{jk}^{(c)}$.

Then,

$$\sum_{j=1}^{N} V_{ij}^{(c)} \sum_{k=1}^{N} \bar{\mathscr{L}}_{jk}^{(e)} \delta x_{1k} = \sum_{j=1}^{N} \sum_{k=1}^{N} \sum_{r=1}^{N} V_{ij}^{(c)} V_{rj}^{(e)} \gamma_r^{(e)} V_{rk}^{(e)} \delta x_{1k} = \sum_{j=1}^{N} \sum_{k=1}^{N} \sum_{r=1}^{N} \sum_{l=1}^{N} V_{ij}^{(c)} V_{rj}^{(e)} \gamma_r^{(e)} V_{rk}^{(e)} V_{lk}^{(c)} \xi_{1l}^{(x)}$$

$$= \sum_{r=1}^{N} \sum_{l=1}^{N} \left[\left\{ \sum_{j=1}^{N} V_{ij}^{(c)} V_{rj}^{(e)} \right\} \gamma_r^{(e)} \left\{ \sum_{k=1}^{N} V_{rk}^{(e)} V_{lk}^{(c)} \right\} \xi_{1l}^{(x)} \right] = \sum_{r=1}^{N} \sum_{l=1}^{N} \left\{ U_{ri}^{(e)} \gamma_r^{(e)} U_{rl}^{(e)} \right\} \xi_{1l}^{(x)}. \tag{15}$$

Using the results of (12), (14), and (15) in (11),

$$\dot{\xi}_{1i}^{(x)} = f_x(x_1, y_1, z_1)\xi_{1i}^{(x)} + f_y(x_1, y_1, z_1)\xi_{1i}^{(y)} + f_z(x_1, y_1, z_1)\xi_{1i}^{(z)} - \epsilon \sum_{r=1}^{N} \sum_{l=1}^{N} \left\{ U_{ri}^{(e)} \gamma_r^{(e)} U_{rl}^{(e)} \right\} \xi_{1l}^{(x)} - g_c \Gamma(x_1)\xi_{1i}^{(x)}$$

$$+ g_c(v_s - x_1)\Gamma_x(x_1)\xi_{1i}^{(x)} - \frac{g_c}{k_c}(v_s - x_1)\Gamma_x(x_1)\gamma_i^{(c)}\xi_{1i}^{(x)} + \eta\left(\xi_{2i}^{(x)} - \xi_{1i}^{(x)}\right). \tag{16}$$

Now, the two Laplacian matrices commute with each other so they can be simultaneously diagonalizable by a common basis of eigenvectors, i.e., $V^{(e)} = V^{(c)}$. So $U^{(e)} = V^{(e)^{tr}} V^{(c)} = V^{(e)^{tr}} V^{(e)} = I_N \Rightarrow U_{ij}^{(e)} = \delta_j^i$. In this case, $\sum_{j=1}^{N} V_{ij}^{(c)} \sum_{k=1}^{N} \bar{\mathscr{L}}_{jk}^{(e)} \delta x_{1k} = \sum_{r=1}^{N} \sum_{l=1}^{N} \{\delta_i^r \gamma_r^{(e)} \delta_l^i\} \xi_{1l}^{(x)} = \gamma_i^{(e)} \xi_{1i}^{(x)}$. Then projecting the error vector $(\delta x_{1i}, \delta y_{1i}, \delta z_{1i})$ on to the basis of eigenvectors, we can

write the master stability equation (MSE) for intralayer synchronization of layer-1 as

$$\begin{aligned}
\dot{\xi}_{1i}^{(x)} &= f_x(x_1, y_1, z_1)\xi_{1i}^{(x)} + f_y(x_1, y_1, z_1)\xi_{1i}^{(y)} + f_z(x_1, y_1, z_1)\xi_{1i}^{(z)} - \epsilon\gamma_i^{(e)}\xi_{1i}^{(x)} - g_c\Gamma(x_1)\xi_{1i}^{(x)} \\
&\quad + g_c(v_s - x_1)\Gamma_x(x_1)\xi_{1i}^{(x)} - \frac{g_c}{k_c}(v_s - x_1)\Gamma_x(x_1)\gamma_i^{(c)}\xi_{1i}^{(x)} + \eta\big(\xi_{2i}^{(x)} - \xi_{1i}^{(x)}\big), \\
\dot{\xi}_{1i}^{(y)} &= g_x(x_1, y_1, z_1)\xi_{1i}^{(x)} + g_y(x_1, y_1, z_1)\xi_{1i}^{(y)} + g_z(x_1, y_1, z_1)\xi_{1i}^{(z)}, \\
\dot{\xi}_{1i}^{(z)} &= h_x(x_1, y_1, z_1)\xi_{1i}^{(x)} + h_y(x_1, y_1, z_1)\xi_{1i}^{(y)} + h_z(x_1, y_1, z_1)\xi_{1i}^{(z)}, \quad i = 1, 2, \ldots, N.
\end{aligned} \tag{17}$$

Similarly, the projecting MSE for layer-2,

$$\begin{aligned}
\dot{\xi}_{2i}^{(x)} &= f_x(x_2, y_2, z_2)\xi_{2i}^{(x)} + f_y(x_2, y_2, z_2)\xi_{2i}^{(y)} + f_z(x_2, y_2, z_2)\xi_{2i}^{(z)} - \epsilon\gamma_i^{(e)}\xi_{2i}^{(x)} - g_c\Gamma(x_2)\xi_{2i}^{(x)} \\
&\quad + g_c(v_s - x_2)\Gamma_x(x_2)\xi_{2i}^{(x)} - \frac{g_c}{k_c}(v_s - x_2)\Gamma_x(x_2)\gamma_i^{(c)}\xi_{2i}^{(x)} + \eta\big(\xi_{1i}^{(x)} - \xi_{2i}^{(x)}\big), \\
\dot{\xi}_{2i}^{(y)} &= g_x(x_2, y_2, z_2)\xi_{2i}^{(x)} + g_y(x_2, y_2, z_2)\xi_{2i}^{(y)} + g_z(x_2, y_2, z_2)\xi_{2i}^{(z)}, \\
\dot{\xi}_{2i}^{(z)} &= h_x(x_2, y_2, z_2)\xi_{2i}^{(x)} + h_y(x_2, y_2, z_2)\xi_{2i}^{(y)} + h_z(x_2, y_2, z_2)\xi_{2i}^{(z)}, \quad i = 1, 2, \ldots, N.
\end{aligned} \tag{18}$$

The direction of the eigenvector corresponding to the zero eigenvalue is parallel to the synchronization manifold, and the other eigenvectors are for transverse directions. The partial derivatives are evaluated as $f_x = -3ax^2 + 2bx,\ f_y = 1,\ f_z = -1;\ g_x = -2dx,\ g_y = -1,\ g_z = 0$, and $h_x = rs, h_y = 0, h_z = -r$. Finally our required MSEs transverse to the synchronization manifold can be written as for layer-1

$$\begin{aligned}
\dot{\xi}_{1i}^{(x)} &= \big(-3ax_1^2 + 2bx_1\big)\xi_{1i}^{(x)} + \xi_{1i}^{(y)} - \xi_{1i}^{(z)} - \frac{g_c\xi_{1i}^{(x)}}{1 + \exp(\lambda(\Theta_s - x_1))} - \epsilon\gamma_i^{(e)}\xi_{1i}^{(x)} \\
&\quad + \frac{g_c}{k_c}(v_s - x_1)\frac{\lambda\exp(\lambda(\Theta_s - x_1))}{[1 + \exp(\lambda(\Theta_s - x_1))]^2}\big[k_c\xi_{1i}^{(x)} - \gamma_i^{(c)}\xi_{1i}^{(x)}\big] + \eta\big(\xi_{2i}^{(x)} - \xi_{1i}^{(x)}\big), \\
\dot{\xi}_{1i}^{(y)} &= -2dx\xi_{1i}^{(x)} - \xi_{1i}^{(y)}, \quad \dot{\xi}_{1i}^{(z)} = r\big(s\xi_{1i}^{(x)} - \xi_{1i}^{(z)}\big),
\end{aligned} \tag{19}$$

and for layer-2

$$\begin{aligned}
\dot{\xi}_{2i}^{(x)} &= \big(-3ax_2^2 + 2bx_2\big)\xi_{2i}^{(x)} + \xi_{2i}^{(y)} - \xi_{2i}^{(z)} - \frac{g_c\xi_{2i}^{(x)}}{1 + \exp(\lambda(\Theta_s - x_2))} - \epsilon\gamma_i^{(e)}\xi_{2i}^{(x)} \\
&\quad + \frac{g_c}{k_c}(v_s - x_2)\frac{\lambda\exp(\lambda(\Theta_s - x_2))}{[1 + \exp(\lambda(\Theta_s - x_2))]^2}\big[k_c\xi_{2i}^{(x)} - \gamma_i^{(c)}\xi_{2i}^{(x)}\big] + \eta\big(\xi_{1i}^{(x)} - \xi_{2i}^{(x)}\big), \\
\dot{\xi}_{2i}^{(y)} &= -2dx\xi_{2i}^{(x)} - \xi_{2i}^{(y)}, \quad \dot{\xi}_{2i}^{(z)} = r\big(s\xi_{2i}^{(x)} - \xi_{2i}^{(z)}\big),
\end{aligned} \tag{20}$$

where $i = 2, 3, \ldots, N$. Here (x_1, y_1, z_1) and (x_2, y_2, z_2) be the state variables of the synchronization manifolds for layer-1 and layer-2 respectively, obeying

$$\begin{aligned}
\dot{x}_1 &= y_1 - ax_1^3 + bx_1^2 - z_1 + I + g_c(v_s - x_1)\Gamma(x_1) \\
&\quad + \eta(x_2 - x_1), \\
\dot{y}_1 &= c - dx_1^2 - y_1, \\
\dot{z}_1 &= r(s(x_1 - x_0) - z_1), \\
\dot{x}_2 &= y_2 - ax_2^3 + bx_2^2 - z_2 + I + g_c(v_s - x_2)\Gamma(x_2) \\
&\quad + \eta(x_1 - x_2), \\
\dot{y}_2 &= c - dx_2^2 - y_2, \\
\dot{z}_2 &= r(s(x_2 - x_0) - z_2).
\end{aligned} \tag{21}$$

Now we calculate all the Lyapunov exponents of the two three-dimensional systems (19) and (20) separately for $i = 2, 3, \ldots, N$. So corresponding to both the layers, we will get two different sets of $(3N - 3)$ Lyapunov exponents for the transverse direction of the intralayer synchronization manifold. From these two different sets, let $\lambda_{\max}^{(1)}$ and $\lambda_{\max}^{(2)}$ be the maximum Lyapunov exponents of layer-1 and layer-2, respectively. Now intralayer synchronization resembles with the complete synchronization of both the two layers. So it will happen if and only if $\lambda_{\max}^{(1)} < 0$ and $\lambda_{\max}^{(2)} < 0$, i.e., $MLE_{\text{intra}} = \max\{\lambda_{\max}^{(1)}, \lambda_{\max}^{(2)}\}$ is negative. The variation of MLE_{intra} by changing the synaptic strengths ϵ, g_c, and η gives the necessary and sufficient conditions for the stability of the intralayer synchronization state when $MLE_{\text{intra}} < 0$. The maximum Lyapunov exponent (MLE) of the MSE given in Eqs. (19), (20), as a function of the parameters ϵ, g_c, and η, gives the necessary condition for the stability of the intralayer synchronous solution. For the synchronous state to be stable, perturbation along all the transverse directions must die out, i.e., the values of MLE should be negative. When the least stable transversal mode associated with the eigenvalue λ_2 is stable, all other transversal modes remain stable.

B. Interlayer synchronization

Now when the interlayer synchronization occurs, let $[\delta x_i(t), \delta y_i(t), \delta z_i(t)]$ be the small perturbation of the ith replica from it's synchronization manifold $[\delta x_{1i}(t), \delta y_{1i}(t), \delta z_{1i}(t)] = [\delta x_{2i}(t), \delta y_{2i}(t), \delta z_{2i}(t)] = [\delta x_i(t), \delta y_i(t), \delta z_i(t)]$, for $i = 1, 2, \ldots, N$. The dynamics of the error vector $(\delta x_i, \delta y_i, \delta z_i)$ near the interlayer synchronization manifold becomes,

$$\begin{aligned}
\dot{\delta x_i} &= \dot{x}_{2i} - \dot{x}_{1i} = f_x(x_i, y_i, z_i)\delta x_i + f_y(x_i, y_i, z_i)\delta y_i + f_z(x_i, y_i, z_i)\delta z_i - \epsilon \sum_{j=1}^{N} \bar{\mathscr{L}}_{ij}^{(e)} \delta x_j \\
&\quad + \frac{g_c}{k_c}(v_s - x_i) \sum_{j=1}^{N} \bar{\mathscr{A}}_{ij}^{(c)} \Gamma_x(x_j)\delta x_j - \frac{g_c}{k_c}\delta x_i \sum_{j=1}^{N} \bar{\mathscr{A}}_{ij}^{(c)} \Gamma(x_j) - 2\eta \delta x_i, \\
\dot{\delta y_i} &= \dot{y}_{2i} - \dot{y}_{1i} = g_x(x_i, y_i, z_i)\delta x_i + g_y(x_i, y_i, z_i)\delta y_i + g_z(x_i, y_i, z_i)\delta z_i, \\
\dot{\delta z_i} &= \dot{z}_{2i} - \dot{z}_{1i} = h_x(x_i, y_i, z_i)\delta x_i + h_y(x_i, y_i, z_i)\delta y_i + h_z(x_i, y_i, z_i)\delta z_i, \quad i = 1, 2, \ldots, N.
\end{aligned} \tag{22}$$

Putting the values of all partial derivatives, we get our required MSF for interlayer synchronization as

$$\begin{aligned}
\dot{\delta x_i} &= \left(-3ax_i^2 + 2bx_i\right)\delta x_i + \delta y_i - \delta z_i - \epsilon \sum_{j=1}^{N} \bar{\mathscr{L}}_{ij}^{(e)} \delta x_j \\
&\quad + \frac{g_c}{k_c}(v_s - x_i) \sum_{j=1}^{N} \bar{\mathscr{A}}_{ij}^{(c)} \frac{\lambda \exp[\lambda(\Theta_s - x_j)]}{\{1 + \exp[\lambda(\Theta_s - x_j)]\}^2} \delta x_j \\
&\quad - \frac{g_c}{k_c}\delta x_i \sum_{j=1}^{N} \bar{\mathscr{A}}_{ij}^{(c)} \frac{1}{1 + \exp[\lambda(\Theta_s - x_j)]} - 2\eta\, \delta x_i, \\
\dot{\delta y_i} &= -2d x_i\, \delta x_i - \delta y_i, \\
\dot{\delta z_i} &= rs\, \delta x_i - r\, \delta z_i, \quad i = 1, 2, \ldots, N,
\end{aligned} \tag{23}$$

where the dynamics of the synchronized manifolds are

$$\begin{aligned}
\dot{x}_{1i} &= y_i - ax_i^3 + bx_i^2 - z_i + I - \epsilon \sum_{j=1}^{N} \bar{\mathscr{L}}_{ij}^{(e)} x_j \\
&\quad + \frac{g_c}{k_c}(v_s - x_i) \sum_{j=1}^{N} \bar{\mathscr{A}}_{ij}^{(c)} \frac{1}{1 + \exp[\lambda(\Theta_s - x_j)]}, \\
\dot{y}_{1i} &= c - dx_i^2 - y_i, \\
\dot{z}_{1i} &= r[s(x_i - x_0) - z_i], \quad i = 1, 2, \ldots, N.
\end{aligned} \tag{24}$$

For $\eta = 0$ the Eq. (23) becomes the linearized equation of the interlayer synchronization manifold (24). Then the directions of all $3N$ Lyapunov exponents of (23) are parallel to the synchronized manifold. For $\eta \neq 0$, all the directions of $3N$ Lyapunov exponents will be transverse to it. The maximum of those exponents (MLE_{inter}) as a function of the parameters (ϵ, g_c, η) actually gives the necessary condition for the stability of the interlayer synchronous solution. Whenever $MLE_{\text{inter}} < 0$, the perturbations transverse to that manifold die out, and all the replicas will evolves in unison. So the negativity of the maximum Lyapunov exponent MLE_{inter} obtained from linearized Eq. (23) together with nonlinear Eq. (24) implies stable interlayer synchronization.

The variation of MLE_{intra} is shown in the color-coded Fig. 10(a) for the parameter space of (ϵ, η) by systematically varying chemical synaptic strength as $g_c = \frac{\epsilon}{2}$ and fixed $k_e = 6$, $k_c = 5$, $p = 0.125$. Here the color bar shows the variation of MLE in which the colors below 0 value signifies the synchronous state. The region of the zero synchronization error [cf. Fig. 3(c)] of the dynamic network for $f \in [10, 100]$ and the region of negative MLE for the time-averaged network are almost identical. So the linear stability analysis of the time-averaged network exactly matches with the numerical results of time-varying networks for sufficiently fast switching (with $f \geqslant 10$). The bottom figure of Fig. 10 represents the variation of MLE_{inter} for interlayer synchronization with respect to the interlayer coupling strength η for fixed values of intralayer coupling strength $\epsilon = 1.8$, and $g_c = \frac{\epsilon}{2}$. Here MSF crosses the 0 line at $\eta \approx 0.58$, which is excellently matched with the higher rewiring frequency for the interlayer synchronization case [cf. Fig. 3(f)]. Here the results for both types of synchronization states are drawn analytically using linear stability analysis and perfectly match with the results of numerical simulations.

VI. DYNAMICAL ROBUSTNESS: STOCHASTIC DEMULTIPLEXING

This section is devoted for the robustness of interlayer synchronization against the stochastic demultiplexing of the

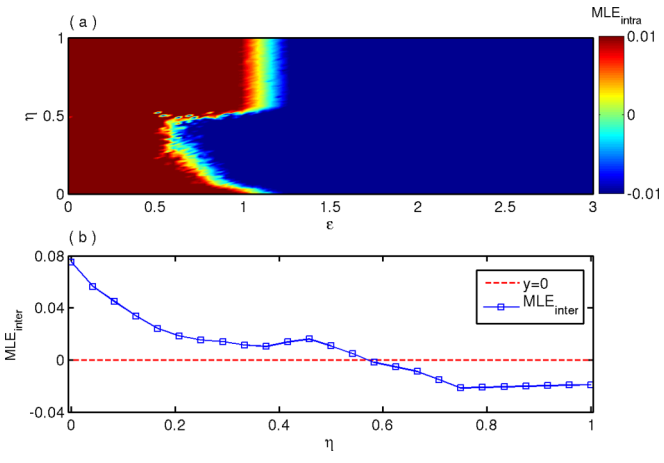

FIG. 10. Variation of maximum Lyapunov exponent corresponding to (a) intralayer synchronization for parameter space (ϵ, η) and (b) interlayer synchronization with respect to the parameter η where $\epsilon = 1.8$. Other parameters: $g_c = \frac{\epsilon}{2}$, $k_e = 6$, $k_c = 5$, and $p = 0.125$.

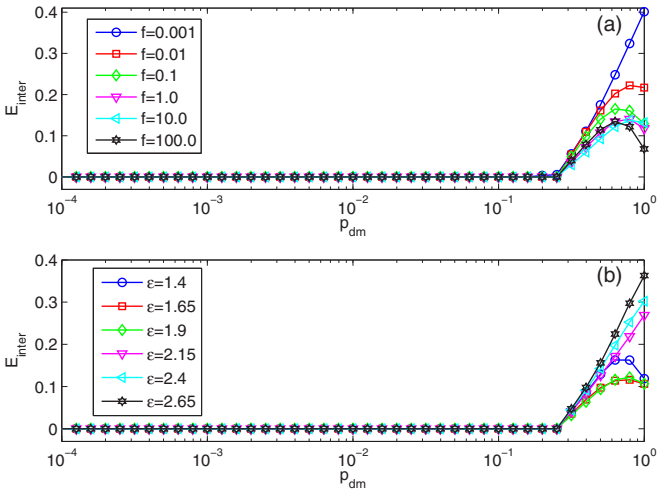

FIG. 11. The variation of the interlayer synchronization error E_{inter} with respect to the demultiplexed probability p_{dm} (a) with fixed $\epsilon = 2.0$, $g_c = \frac{\epsilon}{2}$ and different intralayer rewiring frequencies f, (b) with fixed $f = 1.0$ and varied intralayer coupling strength ϵ, g_c. Other parameters: $\eta = 0.8$, $N = 200$, and $p = 0.125$.

multiplex network. Previously, the robustness of interlayer synchronization was investigated under progressive demultiplexing [28,30], which means, starting from a complete multiplex structure, successive removal of the link between the multiplexed nodes, until the two layers become completely disconnected. Here we explore the stochastic demultiplexing technique, which is defined as the link between any two replica's node is removed with a characteristic probability p_{dm} in each time step. That is, if a multiplex structure of two layers consist of N interlayer connections then the removal of the links with probability p_{dm} refers to the Np_{dm} number of links that are demultiplexed between the layers at that time. In the next time, we again demultiplex each replica with probability p_{dm} from the original multiplex network, i.e., when all the interlayer links are present. So this demultiplexing occurs stochastically and independently for different time step, this fact inspire us to coin the term stochastic demultiplexing. This type of demultiplexed effect is very often in nature and many biological systems. For instance, the social interaction between two different populations are created, destroyed, and rewired over time. In the interneuronal communications, the interaction patterns between two groups of neurons always vary with time. From the ecological perspective, the multilayer organization is the best way to represent the ecological network [63]. The different types of interactions among the various patches are varied with respect to time due to several ecological processes. There are two probabilities in this case, namely the probability for rewiring intralayer network and the probability of demultiplexing replicas.

Figure 11(a) shows the variation of the interlayer synchronization error E_{inter} with respect to the demultiplex probability p_{dm} by considering the several rewiring frequencies f of the intralayer interactions and a fixed intracoupling strength $\epsilon = 2.0$ and $g_c = \frac{\epsilon}{2}$. Similarly, keeping fixed rewiring frequency $f = 1.0$, and taking various intralayer coupling strengths ϵ and $g_c = \frac{\epsilon}{2}$, the interlayer synchronization error is drawn in Fig. 11(b). From this figure, it is observed that for both the cases, the interlayer synchronization persists up to a certain critical value of $p_{dm} = 0.275$. This feature indicates that the robustness of the interlayer synchronization is quite independent of the temporal variation of the intralayer connection and intralayer interaction strength in the stochastic demultiplexing process. This is the sharp contrast with the previous studied of deterministic demultiplexed effect [30] that fast switching of the intralayer connection and the sufficient strong intracoupling strength is favorable to the interlayer synchronization against the large fraction of demultiplexed nodes.

Now to analyze this phenomenon mathematically, we consider the interlayer coupling term of Eq. (1) (third term) as

$$\eta \sum_{j=1}^{N} B_{ij}(t) H(\mathbf{x}_i, \mathbf{y}_i), \tag{25}$$

where η be the interlayer coupling strength, H be the interlayer coupling function and $B(t)$ is the interlayer adjacency matrix determining interlayer coupling topology. Here $B_{ij}(t) = 1$ if the ith node of layer-1 is connected to the jth node of layer-2 at time t, and 0 otherwise. Here, like the intralayer adjacency matrix, the diagonal elements of $B(t)$ may not be 0. In fact for complete multiplex network, $B(t)$ is a diagonal matrix with each diagonal term 1. Now p_{dm} is the probability that there will be no connection between the ith node of layer-1 and ith node of layer-2 at time instant t. So $1 - p_{dm}$ is the probability of there will be a link between the ith replica of the two layers. So the time-averaged interlayer adjacency matrix $\bar{B}$ is

$$\begin{aligned} \bar{B} &= \frac{1}{T}\int_{t}^{t+T} B(\tau)d\tau \\ &= \text{diag}\{\underbrace{1 - p_{dm}, 1 - p_{dm}, \ldots, 1 - p_{dm}}_{N\textbf{times}}\}. \end{aligned} \tag{26}$$

So the term (25) becomes

$$\eta \sum_{j=1}^{N} \bar{B}_{ij}(t) H(\mathbf{x}_i, \mathbf{y}_i) = \eta(1 - p_{dm}) H(\mathbf{x}_i, \mathbf{y}_i). \tag{27}$$

From above it is clear that the time-averaged system is the same as the time static complete multiplex network with effective coupling strength $\eta(1 - p_{dm})$.

Now if $\eta = \eta_0$ is the critical interlayer coupling strength for interlayer synchronization, then for the stochastic demultiplex network, the condition of interlayer coherency is

$$\eta(1 - p_{dm}) \geqslant \eta_0. \tag{28}$$

For fixed value $\eta = 0.8$ and from Fig. 3 interlayer synchrony appears at the interlayer strength $\eta_0 \simeq 0.58$. So for stochastic demultiplexing, the interlayer synchrony sustains if $p_{dm} \leqslant 1 - \frac{\eta_0}{\eta}$, i.e., $p_{dm} \leqslant 0.275$, which excellently matches with our numerical simulation.

VII. CONCLUSIONS

In conclusion, we have investigated the stability of the intralayer and interlayer neuronal synchronization in a

mathematical frame work of the multiplex time-varying neuronal hypernetwork. Here each layer of the multiplex structure presents a hypernetwork, coexistence of two different network topologies with corresponding two different interaction functions in the coupled network. Our considered neuronal hypernetwork structure is modeled through Hindmarsh-Rose neuron model with two different types of synaptic communications, namely chemical synaptic interaction and electrical gap junctional coupling. Since the chemical interaction happened unidirectionally and electrical interaction is bidirectional, so in our proposed neuronal network, we considered the network corresponding to the electrical coupling form a small-world network and chemical interaction is associated with the unidirectional random network. The links in the both types of network structures in each layer are allowed to vary stochastically over time with a characteristic rewiring frequency f with static interlayer interaction. Through the linear stability analysis, we analytically derived the necessary condition of both intralayer and interlayer synchronization states and have excellent matches with the numerical findings. We found that rapid switching of the links in intralayer connection enhanced both the intralayer and interlayer synchronization. Using the basin stability framework, we quantify the stability of these two types of synchronous states in global sense. Further, we estimate the time taken to reach the intralayer and interlayer synchrony in the time-varying neuronal network. Finally, we explored the robustness of the interlayer synchronization state under stochastically demultiplexing of the replica's node in the multiplex network. Interestingly, we observed that this synchronous state is independent of intralayer rewiring frequency and coupling strength. So, the temporal variation of each of the layers in multiplex network has no effect on interlayer synchronization under stochastic demultiplexing. Our findings are expected to give a better understanding of several phenomena in neuronal hypernetworks. The proposed study on neuronal synchronization using time-varying hypernetwork is closely related to the epileptic seizures [64] in the brain dynamics. We believe that there may be some scopes that can help to analyze the multichannel EEG [65,66] recorded neuronal brain activity with the nonlinear time series analysis of the neuronal network.

ACKNOWLEDGMENTS

D.G. was supported by the Department of Science and Technology, Government of India (Project No. EMR/2016/001039).

[1] S. Boccaletti, G. Bianconi, R. Criado, C. I. del Genio, J. Gómez-Gardeñes, M. Romance, I. Sendiña-Nadal, Z. Wang, and M. Zanin, Phys. Rep. **544**, 1 (2014).
[2] M. Kivelä, A. Arenas, M. Barthelemy, J. P. Gleeson, Y. Moreno, and M. A. Porter, J. Complex Net. **2**, 203 (2014).
[3] G. Bianconi, *Multilayer Networks: Structure and Function* (Oxford University Press, Oxford, 2018).
[4] A. Cardillo, J. Gómez-Gardeñes, M. Zanin, M. Romance, D. Papo, F. del Pozo, and S. Boccaletti, Sci. Rep. **3**, 1344 (2013); A. Halu, S. Mukherjee, and G. Bianconi, Phys. Rev. E **89**, 012806 (2014).
[5] M. Szell, R. Lambiotte, and S. Thurner, Proc. Natl. Acad. Sci. U.S.A. **107**, 13636 (2010).
[6] R. Criado, M. Romance, and M. Vela-Pérez, Int. J. Bifurcation Chaos **20**, 877 (2010); R. Criado, B. Hernández-Bermejo, and M. Romance, *ibid.* **17**, 2289 (2007).
[7] A. Cardillo, M. Zanin, J. Gómez-Gardeñes, M. Romance, A. García del Amo, and S. Boccaletti, Eur. Phys. J.: Spec. Top. **215**, 23 (2013).
[8] B. Bentley, R. Branicky, C. L. Barnes, Y. L. Chew, E. Yemini, E. T. Bullmore, P. E. Vértes, and W. R. Schafer, PLoS Comput. Biol. **12**, e1005283 (2016).
[9] B. M. Adhikari, A. Prasad, and M. Dhamala, Chaos **21**, 023116 (2011).
[10] J. J. Crofts, M. Forrester, and R. D. O'Dea, Europhys. Lett. **116**, 18003 (2016).
[11] A. Saumell-Mendiola, M. A. Serrano, and M. Boguñá, Phys. Rev. E **86**, 026106 (2012).
[12] C. Granell, S. Gómez, and A. Arenas, Phys. Rev. Lett. **111**, 128701 (2013).
[13] C. Buono, L. G. Alvarez-Zuzek, P. A. Macri, and L. A. Braunstein, PLoS One **9**, e92200 (2014).
[14] J. Sanz, C.-Y. Xia, S. Meloni, and Y. Moreno, Phys. Rev. X **4**, 041005 (2014).
[15] J. Gao, S. V. Buldyrev, H. E. Stanley, and S. Havlin, Nature Phys. **8**, 40 (2012).
[16] G. Bianconi and S. N. Dorogovtsev, Phys. Rev. E **89**, 062814 (2014).
[17] S. Gómez, A. Díaz-Guilera, J. Gómez-Gardeñes, C. J. Pérez-Vicente, Y. Moreno, and A. Arenas, Phys. Rev. Lett. **110**, 028701 (2013).
[18] Z. Wang, A. Szolnoki, and M. Perc, J. Theor. Biol. **349**, 50 (2014).
[19] G. Menichetti, L. DallAsta, and G. Bianconi, Sci. Rep. **6**, 20706 (2016).
[20] F. Sorrentino, New J. Phys. **14**, 033035 (2012).
[21] A. E. Pereda, Nature Rev. **15**, 250 (2014).
[22] B. L. Partridge and T. J. Pitcher, J. Comput. Phys. **135**, 315 (1980).
[23] N. Abaid and M. Porfiri, J. R. Soc. Interface **7**, 1441 (2010).
[24] C. Zhou, L. Zemanová, G. Zamora, C. C. Hilgetag, and J. Kurths, Phys. Rev. Lett. **97**, 238103 (2006); New J. Phys. **9**, 178 (2007).
[25] S. V. Buldyrev, R. Parshani, G. Paul, H. E. Stanley, and S. Havlin, Nature (London) **464**, 1025 (2010).
[26] A. Pikovsky, J. Kurths, and M. Rosenblum, *Synchronization: A Universal Concept in Nonlinear Sciences*, Cambridge Nonlinear Science Series, Book 12 (Cambridge University Press, Cambridge, 2003).
[27] L. V. Gambuzza, M. Frasca, and J. Gómez-Gardeñes, Europhys. Lett. **110**, 20010 (2015).
[28] R. Sevilla-Escoboza, I. Sendiña-Nadal, I. Leyva, R. Gutiérrez, J. M. Buldú, and S. Boccaletti, Chaos **26**, 065304 (2016).

[29] I. Leyva, R. Sevilla-Escoboza, I. Sendiña-Nadal, R. Gutiérrez, J. M. Buldú, and S. Boccaletti, Sci. Rep. **7**, 45475 (2017).
[30] S. Rakshit, S. Majhi, B. K. Bera, S. Sinha, and D. Ghosh, Phys. Rev. E **96**, 062308 (2017).
[31] S. Jalan and A. Singh, Europhys. Lett. **113**, 30002 (2016).
[32] V. A. Maksimenko, V. V. Makarov, B. K. Bera, D. Ghosh, S. K. Dana, M. V. Goremyko, N. S. Frolov, A. A. Koronovskii, and A. E. Hramov, Phys. Rev. E **94**, 052205 (2016); S. Majhi, M. Perc, and D. Ghosh, Sci. Rep. **6**, 39033 (2016).
[33] X. Zhang, S. Boccaletti, S. Guan, and Z. Liu, Phys. Rev. Lett. **114**, 038701 (2015).
[34] P. Holme and J. Saramäki, Phys. Rep. **519**, 97 (2012).
[35] S. Wasserman, and K. Faust, *Social Network Analysis: Methods and Applications* (Cambridge University Press, Cambridge, 1994).
[36] J. P. Onnela, J. Saramaki, J. Hyvonen, G. Szabo, D. Lazer, K. Kaski, J. Kertesz, and A. L. Barabasi, Proc. Natl. Acad. Sci. U.S.A. **104**, 7332 (2007); Y. Wu, C. Zhou, J. Xiao, J. Kurths, and H. J. Schellnhuber, *ibid.* **107**, 18803 (2010); J. L. Iribarren and E. Moro, Phys. Rev. Lett. **103**, 038702 (2009).
[37] R. Pastor-Satorras and A. Vespignani, *Evolution and Structure of the Internet: A Statistical Physics Approach* (Cambridge University Press, Cambridge, 2004).
[38] I. V. Belykh, V. N. Belykh, and M. Hasler, Physica D **195**, 188 (2004).
[39] V. Kohar, P. Ji, A. Choudhary, S. Sinha, and J. Kurths, Phys. Rev. E **90**, 022812 (2014).
[40] J. Lü and G. Chen, IEEE Trans. Autom. Control **50**, 841 (2005).
[41] M. Frasca, A. Buscarino, A. Rizzo, L. Fortuna, and S. Boccaletti, Phys. Rev. Lett. **100**, 044102 (2008); L. Prignano, O. Sagarra, and A. Díaz-Guilera, *ibid.* **110**, 114101 (2013).
[42] D. Levis, I. Pagonabarraga, and A. Díaz-Guilera, Phys. Rev. X **7**, 011028 (2017).
[43] M. L. Sachtjen, B. A. Carreras, and V. E. Lynch, Phys. Rev. E **61**, 4877 (2000).
[44] V. Kohar and S. Sinha, Chaos Solitons Fractals **54**, 127 (2013).
[45] R. Olfati-Saber, J. A. Fax, and R. M. Murray, Proc. IEEE **95**, 215 (2007).
[46] D. Tanaka, Phys. Rev. Lett. **99**, 134103 (2007).
[47] T. M. Przytycka, M. Singh, and D. K. Slonim, Briefings In Bioinformatics **11**, 15 (2010); S. Lèbre, J. Becq, F. Devaux, M. P. H. Stumpf, and G. Lelandais, BMC Syst. Biol. **4**, 130 (2010); A. Rao, A. O. Hero, D. J. States, and J. D. Engel, EURASIP J. Bioinform. Syst. Biol. **2007**, 51947 (2007).
[48] M. Valencia, J. Martinerie, S. Dupont, and M. Chavez, Phys. Rev. E **77**, 050905(R) (2008).
[49] S. Rakshit, B. K. Bera, D. Ghosh, and S. Sinha, Phys. Rev. E **97**, 052304 (2018).
[50] P. J. Uhlhaas and W. Singer, Neuron **52**, 155 (2006).
[51] R. Bartsch, J. W. Kantelhardt, T. Penzel, and S. Havlin, Phys. Rev. Lett. **98**, 054102 (2007).
[52] W. Singer and C. M. Gray, Annu. Rev. Neurosci. **18**, 555 (1995).
[53] R. Llinas and U. Ribary, Proc. Natl. Acad. Sci. U.S.A. **90**, 2078 (1993).
[54] D. K. Hartline, Biol. Cybern. **33**, 223 (1979).
[55] C. I. Del Genio, J. Gómez-Gardeñes, I. Bonamassa, and S. Boccaletti, Sci. Adv. **2**, e1601679 (2016).
[56] P. J. Menck, J. Heitzig, N. Marwan, and J. Kurths, Nature Phys. **9**, 89-92 (2013).
[57] S. Rakshit, B. K. Bera, M. Perc, and D. Ghosh, Sci. Rep. **7**, 2412 (2017).
[58] S. G. Hormuzdi, M. A. Filippov, G. Mitropoulou, H. Monyer, and R. Bruzzone, Biochim. Biophys. Acta **1662**, 113 (2004).
[59] E. R. Kandel, J. H. Schwartz, and T. M. Jessell, *Principles of Neural Science* (McGraw Hill, New York, 2000).
[60] D. J. Watts and S. H. Strogatz, Nature (London) **393**, 440 (1998).
[61] P. G. Lind, A. Nunes, and J. A. C. Gallas, Physica A **371**, 100 (2006).
[62] D. J. Stilwell, E. M. Bollt, and D. G. Roberson, SIAM J. Appl. Dyn. Syst. **5**, 140 (2006).
[63] S. Pilosof, M. A. Porter, M. Pascual, and S. Kéfi, Nature Ecol. Evol. **1**, 0101 (2017).
[64] V. V. Makarov, V. A. Maximenko, G. van Luijtelaar, A. Lüttjohann, and A. E. Hramov, Proc. SPIE **10493**, 1049311 (2018).
[65] A. Hramov, V. Y. Musatov, A. E. Runnova, T. Y. Efremova, A. A. Koronovskii, and A. N. Pisarchik, Proc. SPIE **10717**, 107171M (2018).
[66] C. J. Stam, Clinical Neurophys. **116**, 2266 (2005).